Research Article | Vol. 11, No. 2 / 1 February 2020 / Biomedical Optics Express 801
Biomedical Optics EXPRESS

Light-assisted drying for anhydrous preservation of biological samples: optical characterization of the trehalose preservation matrix

MADISON A. YOUNG,[1] DANIEL P. FURR,[1] RILEY Q. MCKEOUGH,[1] GLORIA D. ELLIOTT,[2] AND SUSAN R. TRAMMELL[1,*]

[1] University of North Carolina at Charlotte, Department of Physics and Optical Science, Charlotte, NC 28226, USA
[2] University of North Carolina at Charlotte, Department of Mechanical Engineering, Charlotte, NC 28226, USA
[*] srtramme@uncc.edu

Abstract: Protein-based drugs have been developed to treat a variety of conditions and assays use immobilized capture proteins for disease detection. Freeze-drying is currently the standard for the preservation of proteins, but this method is expensive and requires lengthy processing times. Anhydrous preservation in a trehalose amorphous solid matrix offers a promising alternative to freeze-drying. Light assisted drying (LAD) is a processing method to create an amorphous trehalose matrix. Proteins suspended in a trehalose solution are dehydrated using near-infrared laser light. The laser radiation accelerates drying and as water is removed the trehalose forms a protective matrix. In this work, LAD samples are characterized to determine the crystallization kinetics of the trehalose after LAD processing and the distribution of amorphous trehalose in the samples. These characteristics influence the long-term stability of the samples. Polarized light imaging revealed that LAD processed samples are stable against crystallization during low-humidity storage at room temperature. Scanning white light interferometry and Raman spectroscopy indicated that trehalose was present across samples in an amorphous form. In addition, differential scanning microcalorimetry was used to measure the thermodynamic characteristics of the protein lysozyme after LAD processing. These results demonstrate that LAD does not change the properties of this protein.

1. Introduction

The use of protein-based therapeutics and diagnostics has increased dramatically over the past 25 years. Protein-based drugs have been developed to treat diseases ranging from arthritis to psoriasis [1,2]. Laboratory based assays use high-throughput 96-well microtiter plates that contain immobilized capture proteins for the detection of diseases and for monitoring protein levels [3,4]. Protein-based assays have also been developed for rapid, point-of-care diagnostics and newly developed microfluidic devices require the use of protein indicators [5].

A challenge in the development of protein-based products is maintaining the protein in the folded state during processing and storage, as the three-dimensional structure of the protein is often responsible for its functional activity. The most common method of stabilizing proteins for storage and later use is lyophilization (freeze drying). However, the freeze-drying process remains expensive and requires lengthy processing times. In addition, many proteins that are lyophilized still must be refrigerated or frozen to maintain functionality [6–9]. Cold storage strategies can be challenging for the transportation of protein-based products and can be difficult or impossible in low resource settings due to a lack of available infrastructure. An inexpensive, simple processing

#376630 https://doi.org/10.1364/BOE.376630
Journal © 2020 Received 19 Sep 2019; revised 7 Dec 2019; accepted 6 Jan 2020; published 14 Jan 2020

Biomedical Optics EXPRESS

method that enables supra-zero temperature storage of proteins used in therapeutics and assays is needed.

Recent research has demonstrated that anhydrous, or dry state, preservation in a trehalose amorphous (non-crystalline) solid matrix may be an alternative to freeze drying for the preservation of biological samples [10–12]. An amorphous solid restricts molecular motion to a small volume over a finite time period, which can prevent the degradation of biologics, such as proteins, embedded in the matrix. An amorphous solid is a non-crystalline solid in which the atoms and molecules are organized such that there is no long-range order. The regular lattice of a crystalline solid can damage embedded biologics, limiting the usefulness of these solids as preservation matrices. Disaccharide trehalose can form an amorphous solid at room temperature and can also act as a bioprotectant, making trehalose an attractive option as a preservation matrix for embedded biologics [10].

We have previously described a new processing technique, light assisted drying (LAD), to create trehalose amorphous solids for the preservation of biologics [13]. LAD uses illumination by near-infrared laser light to assist in the formation of trehalose amorphous solids. Static air-drying of sugar solutions is dominated by evaporative cooling which causes the drying rate to slow substantially and allows for crystallization of the sugars. LAD selectively heats water to overcome cooling due to evaporation and speeds dehydration of the samples. As water is removed from the sample, the remaining sugars and salts become concentrated, and, as long as the solutes do not crystallize, the viscosity increases with progressive water loss until an amorphous solid is achieved. Because a substantial reduction of molecular mobility is necessary to ensure an extended shelf life, samples generally need to be stored below the glass transition temperature, T_g, of the trehalose matrix to prevent degradation [14]. Below T_g the trehalose maintains its amorphous state. The glass transition temperature for an amorphous trehalose solid formed by dehydration depends on the amount of water remaining in the sample after processing. The more water that remains in the sample, the lower the glass transition temperature. Lower end moisture contents (EMC's) are necessary for storage at higher temperatures.

Other researchers have devised ways to form trehalose amorphous solids for use as preservation matrices. These include drying in controlled humidity desiccators, [15] the use of high flow nitrogen gas for convective drying [16] and microwave-assisted drying [17]. LAD has the benefit of being able to deliver more precise amounts of energy to each sample than these other methods. Precise control over energy deposition means precise control over EMC which dictates sample storage temperature. In addition, LAD could be used for inline processing of assays or drugs.

Our previous work has demonstrated the effectiveness of LAD to reach EMCs low enough for storage at elevated temperatures in the glassy state and determined the optimal LAD processing parameters for achieving these EMCs [13]. In this work, we characterize sample morphology, crystal formation and the distribution of the glass forming matrix in small volume samples processed via LAD. In addition, the effect of LAD processing on the thermodynamic properties of the model protein lysozyme are assessed. Lysozyme was chosen as a test protein for these studies because it is widely available, easy to work with and its structure and thermal properties are well understood.

Polarized light imaging (PLI) was used to locate areas of crystallization and monitor crystallization kinetics of samples during storage in a low relative humidity (RH = 14%) environment [18]. Understanding the crystallization characteristics of samples is important because localized areas of crystallization can act as nucleation points and cause of crystallization of a sample. Crystallization can lead to physical stress on biologics embedded in the matrix [19]. Scanning white light interferometry (SWLI) was used to measure sample thickness and surface morphology after LAD processing and after long term (~1 month) storage at low RH. Variations in thickness across the sample may indicate an uneven distribution of the trehalose preservation matrix which could impact the overall functionality of embedded proteins. Raman spectroscopy was used

Biomedical Optics EXPRESS

in conjunction with SWLI to investigate trehalose distribution across LAD processed samples and to determine if the trehalose was in an amorphous state across the sample. In addition, we have measured the thermodynamic properties of a model protein, lysozyme, immediately after LAD processing using Differential Scanning Calorimetry (DSC). Changes in the thermodynamic properties could indicate that LAD is damaging the protein during processing either thermally or through direct interaction between the laser light and protein.

2. Methods

2.1. LAD processing, sample solution, and sample storage

A schematic of the experimental setup is shown in Fig. 1. An IPG Photonics continuous wave (CW) ytterbium fiber laser at 1064 nm (YLR-5-1064) was used for LAD processing. The source had a maximum power output of 5 W with built in control of power. The laser emits a collimated, single-mode, Gaussian beam with a full width at half maximum (FWHM) spot size of ~4.5 mm which was measured using a BeamTrack 10A-PPS thermal sensor (Ophir Photonics). A FLIR SC655 infrared (IR) camera was used to record the temperature of samples during all processing. Thermal imaging provides a method to noninvasively monitor the sample temperature during processing. The camera (sensitive from 7.5 to 14 microns) has an array of 640×480 pixels and a maximum frame rate of 200 fps. All studies were performed in a humidity-controlled environment that was kept at approximately 11% relative humidity (RH). This was achieved by pumping dry air into a chamber containing the experimental setup as shown in Fig. 1 and monitoring the RH with a temperature and RH logger (ONSET UX100-011).

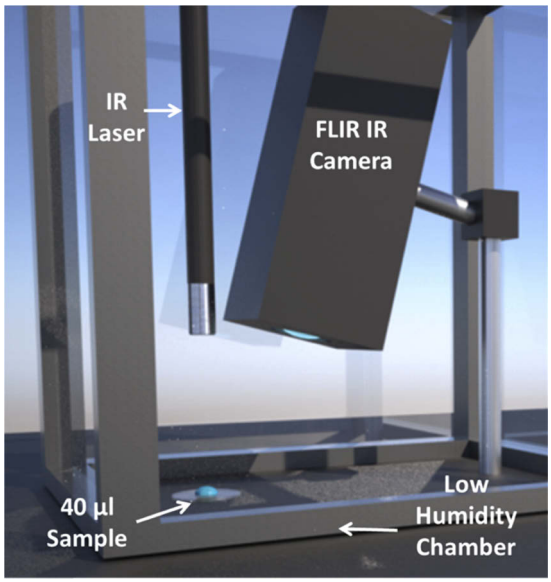

Fig. 1. Experimental set-up of the light-assisted drying (LAD) technique within a controlled low relative humidity chamber. A small volume sample is illuminated with a near-IR laser. The temperature of the sample is monitored during processing using the thermal camera (Ref. [13], Fig. 1).

All samples in the studies consisted of 40 µl droplets containing a model protein, egg white lysozyme (Worthington Biochemical LS002933), dissolved in drying solution (DS) at a concentration of 0.5 mg/ml. This was verified using the absorption of light at 280 nm with a microplate spectrophotometer (Bio-Tek Synergy HT). The DS consisted of 0.2M disaccharide

Biomedical Optics EXPRESS

trehalose in 0.33 x phosphate buffer solution (PBS) [[20]]. The dry weight of the DS was determined through bake out method to be 7.01% the mass of a sample. Dry weight was adjusted to include the mass of the protein based on its concentration to determine the total dry weight.

For each test, a 40 µL droplet of the protein/drying solution was deposited onto a substrate and the initial mass was determined gravimetrically using a balance (RADWAG AS 82/220.R2) accurate to 0.01 mg. The substrates used in these studies were 18 mm diameter borosilicate glass coverslips (Fisherbrand 12-546). The glass cover slips allow for easy recovery and rehydration of the proteins after LAD processing. On the glass coverslips, the samples were droplets roughly 2 mm in thickness with a diameter of approximately 7 mm. A fiducial was marked on the edge of the coverslip to ensure consistent orientation for imaging conducted during this study. The sample was then moved into the humidity chamber for laser irradiation. Samples were processed for 60 minutes at 5 W (26.9 W/cm^2). The maximum temperature of the sample was monitored during processing using the thermal camera. Samples reached a maximum sample temperature of 44.4 ± 0.7 °C during LAD processing. The ambient temperature of the chamber (~23°C) was kept constant during processing. After irradiation, the sample was removed from the humidity chamber and immediately massed again. End moisture content (EMC), which is a measure of the amount of water relative to the dry mass of a sample, was calculated as:

$$EMC = \frac{m_f - m_s - m_{dw}}{m_{dw}} \tag{1}$$

where m_f is the mass of the final sample including the mass of the substrate, m_s, and m_{dw} is the calculated dry weight of the initial sample. All samples in this study were processed to an average EMC of 0.17 ± 0.04 gH_2O/gDryWeight (consistent with our previously reported EMC's for 60 minutes of processing with the 1064-nm laser [13]).

For comparison, 40 µL samples of the same solution were air-dried by placing the samples in the humidity-controlled chamber (~11% RH) for 60 minutes. The EMC's for these samples were calculated using Eq. 1 in the same manner as used for the LAD processed samples. Air-dried samples had an average EMC of 5.11 ± 1.3 gH_2O/gDryWeight after processing. Air drying for 60 minutes did not result in the formation of an amorphous or crystalline trehalose solid.

After processing (LAD or air drying), all samples were stored individually in small volume containers above a saturated salt solution of lithium chloride (LiCl) (ChemCenter). The RH of the LiCl saturated salt was 14.3 ± 0.5% RH (measured with an RH probe HH314A, Omega). Samples were stored at room temperature (~23°C).

2.2. Polarized light imaging

The PLI experimental set-up (Fig. 2) consisted of a white light fiber optic illuminator (41720, Cole Palmer), two linear polarizers (LPVISE050-A, Thorlabs), with the second polarizer acting as an analyzer, and a digital camera (Nikon D100) aligned in the vertical direction. The camera was equipped with a Nikon 28-105mm f/3.5-4.5 lens and manually focused on the image plane. The spatial resolution of the set-up was 10 µm/pixel. LAD samples (N = 8) and air dried samples (N = 4) were processed as described in Sec. 2.1. Immediately after processing, samples were placed on a glass microscope slide in between the polarizers and imaged from above. Two images were taken: the first with the analyzer oriented at 0° to the polarizer and the second with the analyzer oriented at 90° to the polarizer. After initial imaging, the samples were then placed in containers above a LiCl (14.3 ± 0.5% RH) saturated salt solution for storage. Samples were then imaged and massed (to monitor crystal formation and EMC) every 30 minutes for the first two hours in storage, then every hour for the next 2 to 5 hours and once a day until the end of the study.

Biomedical Optics EXPRESS

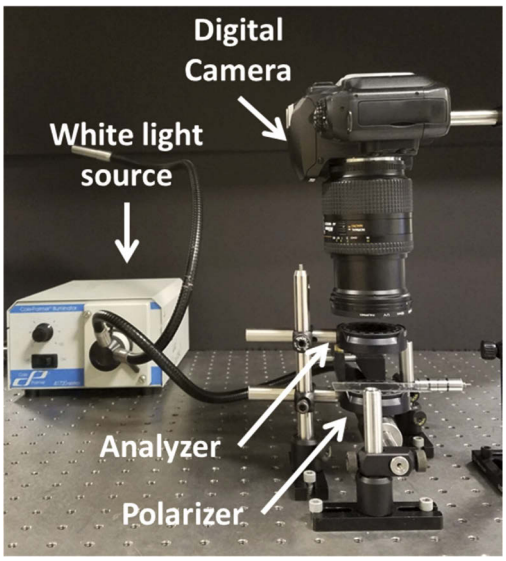

Fig. 2. Polarized light imaging set-up. Samples were placed on a borosilicate glass coverslip between the polarizer and analyzer and then imaged from above.

2.3. Scanning white light interferometry

Sample thickness was measured with a Zygo Nexview Scanning White Light Interferometer (SWLI) with a 2.75X Michelson objective (spatial resolution: 5.88 μm/pixel). Samples (N = 7) were LAD processed (as described in Sec. 2.1) and stored in containers above a LiCl (14.3 ± 0.5% RH) saturated salt solution. Sample surface profiles were measured after one day of storage and then again after 27 days of storage. EMC was measured just prior to all SWLI measurements. The data was exported into Matlab and HDFView for further processing. In Matlab transverse height was displayed as a color map across the sample, the average maximum height of the sample was calculated, and two diagonal cross sections were extracted. The HFView software was used to extract non-interferometric images.

2.4. Raman spectroscopy

Raman spectroscopy was used to measure the Raman shift of trehalose across LAD processed samples. A schematic of the Raman spectroscopy set-up is shown in Fig. 3. The excitation source was a 785 nm laser diode (BeamQ) with a power output of 200 mW. The beam passed through a 100 μm pinhole and 785 notch filter to spatially and spectrally refine the beam. The beam was then expanded and collimated before entering an IX70 inverted microscope (Olympus). A 100X oil immersion objective was used to focus the light onto the sample. Raman signal from the sample was then collected back into the objective lens, directed into a spectrometer (SR-303i-B, Andor) and collected with a CCD camera (DU420A-BR-DD, Andor). The spectral resolution of the system was 0.28 nm/pixel. The center wavelength of the spectra was set to 855.36 nm to exclude the laser line from the spectra. Data was collected at an exposure time of 5 seconds and 60 accumulations to achieve maximum signal to noise.

Samples (N = 5) were LAD processed and stored in containers above a LiCl (14.3 ± 0.5% RH) saturated salt solution as described in Sec. 2.1. After one day of storage EMC was measured and SWLI was performed as described in Sec. 2.3. The following day the Raman spectra were taken at three separate locations across each sample. Each spectrum was background corrected and

Biomedical Optics EXPRESS

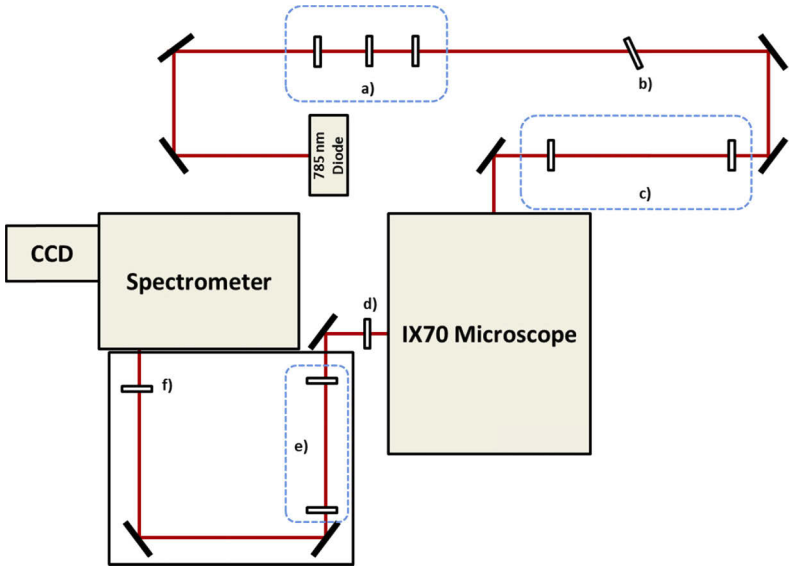

Fig. 3. Raman spectroscopy set-up. The laser beam passes through a) a lens system with a 100 µm pinhole to clean up the intensity profile followed by a b) 785 nm notch filter to spectrally clean up the beam and then an c) expander into the microscope. The Raman signal from the sample exits the microscope and passes through an d) edge filter to remove the excitation wavelength. Then it goes through a e) beam expander and collimator before passing through a f) focusing lens into the spectrometer.

baseline corrected to remove the signal from the coverslip using Andor Solis software. Corrected spectra were exported to Matlab where they were smoothed and normalized to their maximum.

2.5. *Differential scanning calorimetry*

A MicroCal VP-DSC microcalorimeter (MicroCal, Northampton,MA) was used to assess the effect of LAD processing on the thermal stability of the protein lysozyme. For comparison, four samples of lysozyme were tested for unfolding using DSC. Unprocessed lysozyme was used as a control and LAD processed lysozyme was used to determine if laser irradiation caused unfolding of the protein. Air dried samples and samples subjected to a 43°C water bath (the approximate maximum temperature of samples during LAD processing) were also include for comparison.

LAD and air-dried samples were prepared as described in Sec. 2.1 The LAD processed (N = 2) and air-dried (N = 2) samples were rehydrated with deionized water after desiccation for DSC measurement. The resulting concentration due to dilution for all samples was 0.20 mg/ml of lysozyme in 0.085M trehalose and 0.14X PBS. The concentration of the solutions after dilution was measured using a BioTek Synergy HT Microplate reader (BioTek instruments, Winooski, VT). The 43°C water bath (N = 3) samples were 0.20 mg/ml lysozyme in 0.085M trehalose and 0.14X PBS. These samples were placed in a test tube then submerged in a water bath at 43°C for 1 hour. This temperature was similar to the temperatures that samples reached during LAD processing.

DSC baseline repeatability was established with a minimum of 5 reference solution scans (0.085M trehalose in 0.14X PBS). Once a stable baseline was established, the samples containing lysozyme were loaded by syringe into the calorimeter. All scans were carried out at a scan rate of 90°C/hr from 10°C to 90°C with a 15 minute pre-scan equilibration time. The data was analyzed using Origin software provided by MicroCal to determine the midpoint temperature of transition, T_m, and the calorimetric enthalpy of unfolding, ΔH.

Biomedical Optics EXPRESS

3. Results and discussion

3.1. Polarized light imaging: crystallization and end moisture content of samples as a function of storage time

Crystallization occurs as water evaporates from a sugar solution. As the water evaporates the solution saturates and forms a precipitate in the form of a sugar crystal [21]. In order for this to happen the evaporation has to be slow enough that the sugar has time to align itself into its crystalline pattern. The goal of LAD is to speed up evaporation enough so that this does not occur; however, some crystallization may result during processing or form over time as the amorphous solid relaxes. The EMC and crystallization of samples were measured as a function of time. Samples were processed using LAD, the EMC was measured post-processing and then samples were placed in containers at low RH ($14.3 \pm 0.5\%$) and stored at room temperature as described in Sec. 2.1. Air dried samples were stored in the same manner and evaluated for comparison. Figure 4 shows the change in EMC as a function of storage time for LAD processed and air dried samples. We also imaged samples without lysozyme present in the solution. There was no change in the crystal growth in these samples compared to samples containing lysozyme.

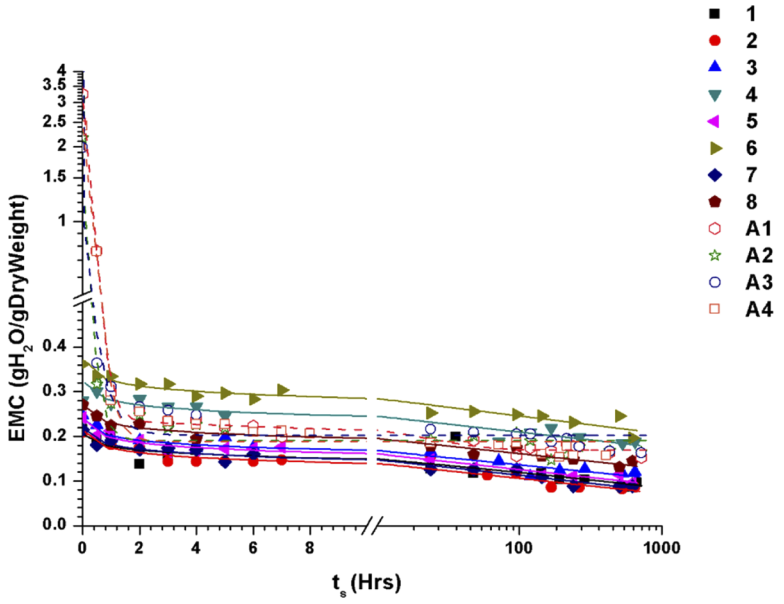

Fig. 4. EMC as a function of storage time for air dried (A1-A4:) and LAD (1-8) processed samples stored at $14.3 \pm 0.5\%$ RH.

A slight decrease in EMC is evident for the LAD processed samples during storage. After approximately 100 hours of storage, LAD processed samples approached their moisture loss limit. All air dried samples showed a significant decrease in moisture content with the highest evaporation rate occurring during the first 3 hours of storage and reached a moisture loss limit after 10 hours. This is not surprising, as these samples had large water content at the beginning of storage. The air dried samples lost moisture through slow evaporation during low humidity storage. The EMC of the LAD processed samples did not change much over the course of storage as they were already very dry when they were placed in the low humidity storage containers.

PLI images were acquired of LAD processed and air dried samples and analyzed in Matlab (R2017B). Each polarized image (image taken with crossed polarizers) was changed to a grayscale intensity image. A threshold intensity for each image was established by finding the average maximum value of intensity of an area outside the sample plus two standard deviations. All

Biomedical Optics EXPRESS

pixels with intensities below the threshold value were zeroed. Crystal area was then measured by the number of pixels with intensity higher than zero in the crossed polarizer image. This measurement was used to determine crystal growth within a sample over time. This was a relative measurement for each sample, not an absolute measurement of crystal area from sample to sample. It is important to note that measured crystal area might include noise from dust and particulates that also polarized light, however this signal was present in all successive images and did not factor into the determination of crystal growth. Figure 5 is an example of the images obtained. Panel a) shows the white light image of the sample and b) the corresponding crossed polarizer image after Matlab processing. The white area is crystallization present in the sample.

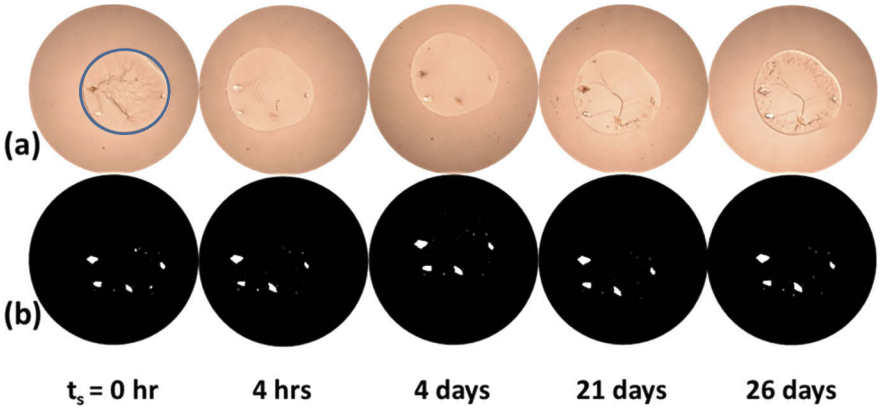

Fig. 5. Time progression of samples stored in LiCl saturated salt low RH containers. The blue circle indicates the sample (7mm diameter), the surrounding area is the coverslip. a) Samples imaged through uncrossed polarizers and b) samples imaged with cross polarizers and processed in Matlab for crystal area measurement. The white area is crystallization present in the sample.

Figure 6 shows the crystal growth as a function of storage time for LAD processed and air dried samples. There is a distinct difference in behavior between the air dried and LAD processed samples. Air dried samples exhibited a significant increase of crystallized area during the first 10 hours of storage, corresponding to the time during which air dried samples experienced an decrease in moisture content. Air dried samples reached a moisture loss limit after 10 hours corresponding to the time at which crystal growth stopped. Again, this result is not surprising. These sample had large moisture content at the beginning of storage and lost moisture through evaporation during low humidity storage. This process resulted in crystallization, as expected. On the other hand, LAD processed samples had low crystal content after processing and experienced negligible crystal growth during storage. One LAD sample (8) contained an uncharacteristically large amount of crystallization (>3000 pixels) post LAD followed by an increase in crystal area. Sample 8's uncharacteristically large initial crystal could have been caused by a particulate in the sample acting as a seed for crystallization.

LAD processed samples remained in the amorphous state when stored at room temperature and low RH. Air-dried samples did reach EMC's comparable to the LAD samples during storage. However, the air dried samples crystalized during drying and storage, while the LAD samples did not experience significant crystal growth.

Imaging of samples revealed other effects in addition to crystallization - wrinkling, and desiccation cracking. Wrinkling of the samples (see Fig. 5(a) for $t_s = 0$ hr) only occurred when samples were removed from low RH environments and placed into the higher RH of the room. When placed back in low RH wrinkling dissipated quickly. This likely resulted from a change in volume at the surface of the sample [22]. The samples mass distribution reached equilibrium

Biomedical Optics EXPRESS

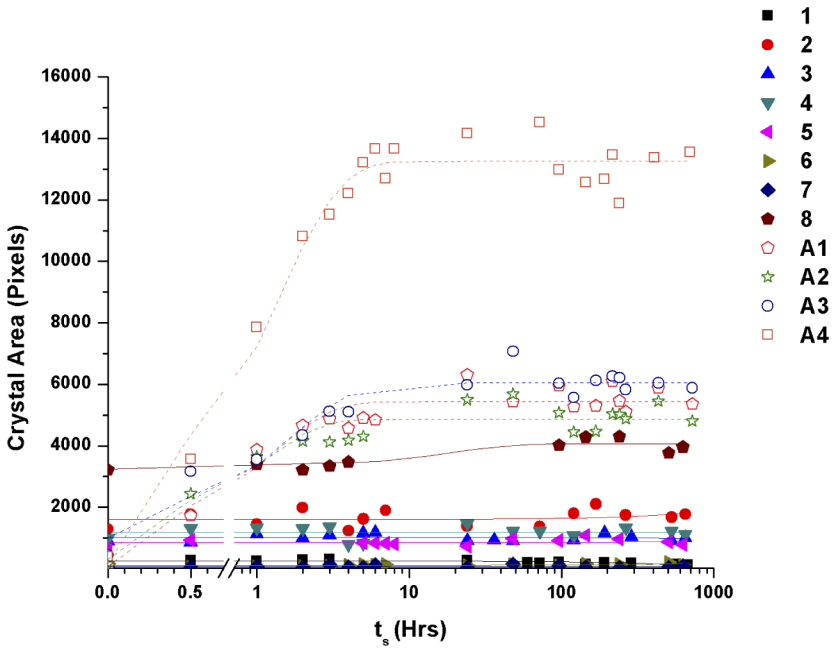

Fig. 6. Crystal area as a function of storage time for air dried (A1-A4) and LAD (1-8) processed samples stored at 14.3 ± 0.5% RH.

while being processed at a low RH. When placed in a higher RH the surface absorbed moisture from the air causing it to superficially swell. The interior of the sample, which was contact pinned to the substrate, was no longer in equilibrium with the surface resulting in wrinkling. LAD processed samples require storage at low RH to prevent the absorption of moisture into the outer layers of the droplet.

Desiccation cracking was observed after storage at low RH (see Fig. 5(a) for $t_s = 26$ days). The average storage time for desiccation cracking to begin for LAD processed samples was t_s=324 ± 159 hours. Cracking was observed beginning on the edge of the drop. This exterior to interior crack formation indicates that a viscous ring was forming on the edge of the droplet and moving inward as the sample continued to dry during low RH storage. The viscous sample at the substrate interface allowed for adhesion while the air interface allowed for evaporation, when these processes competed tensile stresses caused cracks to form [23]. This is in agreement with studies done on cracking of sessile droplets by other groups [24,25]. A flexible substrate could limit or eliminate the desiccation cracking and will be tried in future studies.

3.2. *Scanning white light interferometry: surface profiles and thicknesses of LAD processed samples*

SWLI was used to characterize the topography and thickness of LAD processed samples. Figure 7 shows a color map of sample height. Two cross sections are marked by red and black dashed lines and their corresponding profiles are displayed. The slope of the edges of the samples was outside the range of measurement capable by the Nexview, these areas display as zero height. The coverslip height shown on the edges of the profile was used as the base of the sample and subtracted from sample height to obtain thickness.

The average maximum thickness of LAD processed samples one day after low RH storage was 90.81 ± 6.53 microns with an EMC of 0.16 ± 0.04 gH_2O/gDryWeight. The average decrease in maximum sample thickness after 27 days of low RH storage was 8.65 ± 1.71 microns

Biomedical Optics EXPRESS

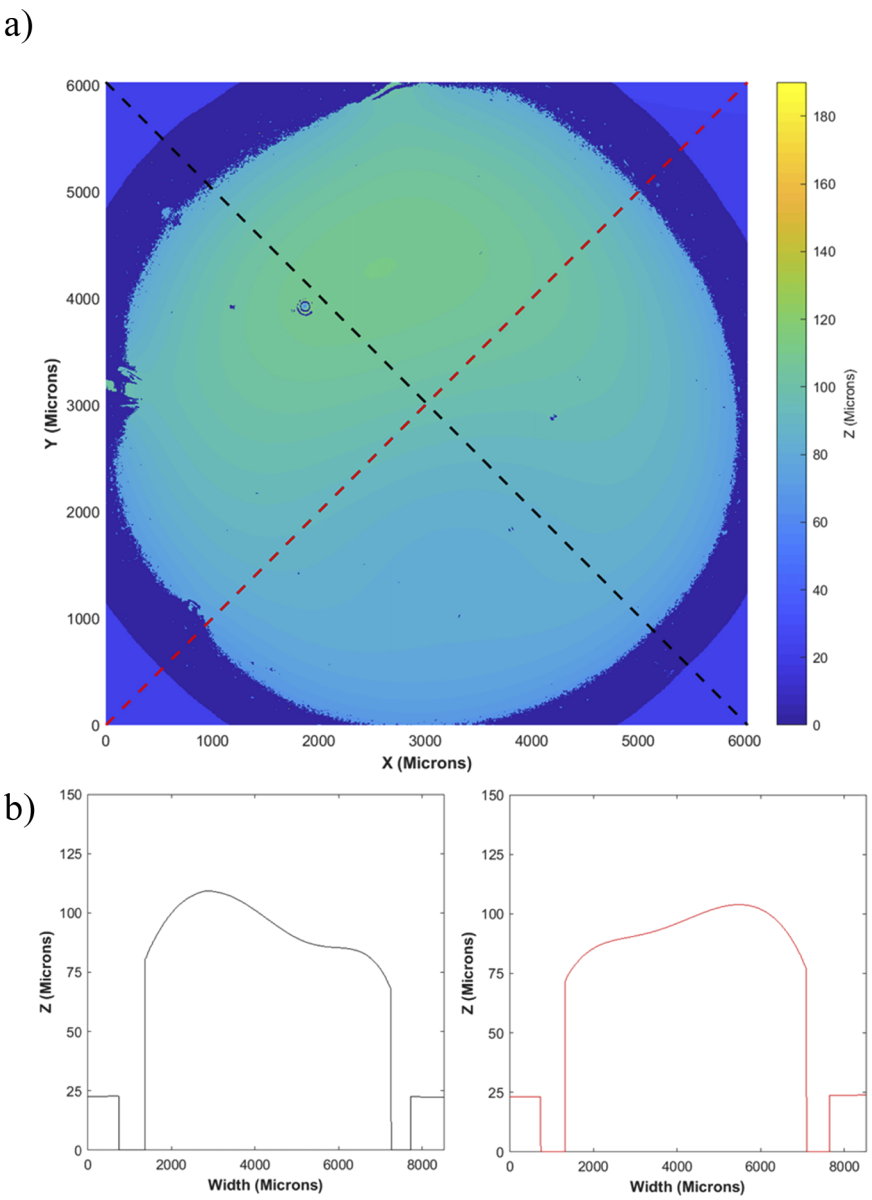

Fig. 7. a) Color map of the height across sample as determine with SWLI, blue and red dashed lines are b) associated cross sections height profiles.

corresponding to a decrease in EMC of 0.04 ± 0.02 $gH_2O/gDryWeight$. There was no statistically significant relationship between a decrease in EMC and a decrease in sample height, most likely because the changes were on such a small scale. We also imaged samples without lysozyme present in the solution. There was no change in thickness or overall morphology of these samples compared with samples containing the protein.

Profiles taken from all samples indicate that there is variability in thickness across the sample. A majority of samples exhibited a dome shape profile with the thickest part of the sample lying slightly off center. A few samples also showed a slight off center dip in the profile. The shape of

Biomedical Optics EXPRESS

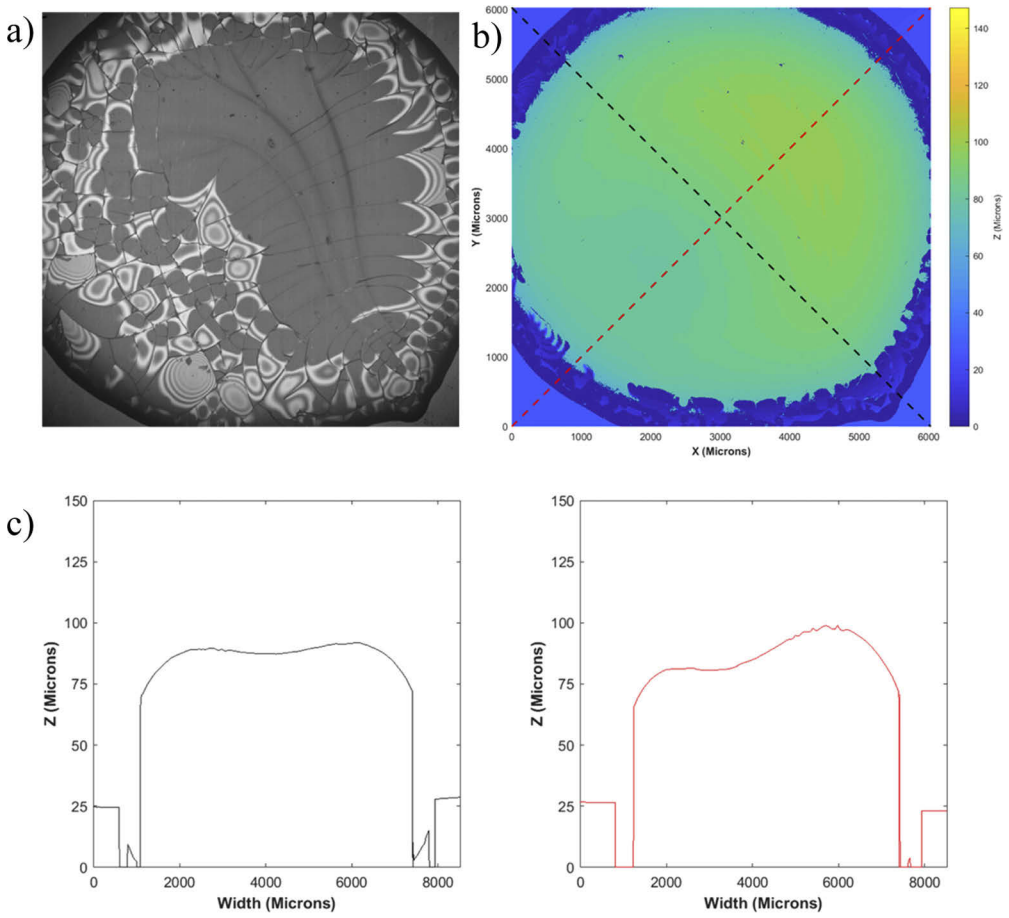

Fig. 8. LAD processed sample after 27 days of storage at 14.3 ± 0.5% RH. a) The non-interferometric image and b) the SWLI height map with corresponding c) height profiles.

the profile did not change during storage just the overall thickness. The off center nature could be from variability of the position of the laser on the sample during processing.

SWLI was also used to determine whether cracking after low RH storage was occurring on the sample/coverslip or sample/air interface. Figure 8 shows a comparison of a SWLI color map, non-interferometric image, and corresponding profiles for a cracked sample. We see in the non-interferometric image that the cracks extend all the way across the sample; however, they do not show up on the height profile. This implies the cracks must be subsurface, on the sample/coverslip interface. This is supported by the fact that we can see white light interference fringes in Fig. 8(a) from the thin air gap that is forming from delamination. Delamination could potentially comprise sample integrity. These results indicate that a different substrate (perhaps more flexible) might be needed to prevent cracking.

3.3. *Raman spectroscopy: distribution of amorphous trehalose in LAD processed samples*

Crystalline trehalose has very well defined, narrow bands while the amorphous bands are broadened (see Fig. 9). Because crystals possess long-range translational symmetry they have quantized lattice vibrations, and this limits the number of Raman active vibrational modes. The

Biomedical Optics EXPRESS

amorphous form does not have spatial order so vibrational modes are not limited by lattice vibrations. This means that all the vibrational modes are sampled resulting in band broadening [26].

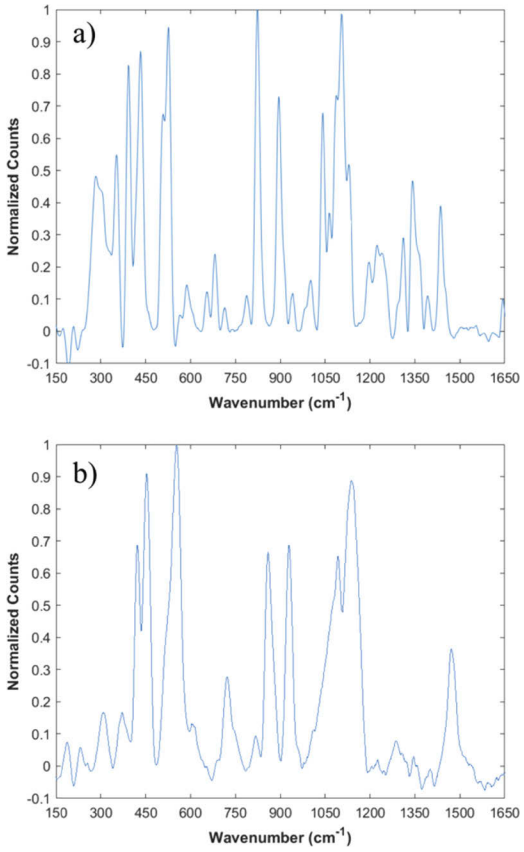

Fig. 9. Raman spectra of a) crystalline trehalose and b) amorphous trehalose acquired with the Raman system described in Sec. 2.4.

Spectra were acquired at three transverse locations across a LAD sample to measure the relative distribution of trehalose across the sample. This was coupled with SWLI of the same sample to determine the relationship between thickness and trehalose distribution. Figure 10 is a SWLI cross section of a sample with the Raman spectra locations marked and the corresponding spectra at each location. First, we note that the Raman spectrum for trehalose is present at each location indicating that the sugar is distributed across the sample. We also see that the trehalose at each location is in the amorphous state and not crystalline. Comparing each sample set of spectra to the corresponding thickness measurement yielded no relationship. No lines from lysozyme are apparent in the Raman spectra with the excitation source used in this study. We obtained Raman spectroscopy of samples without lysosome in the solution. There was no change in the Raman spectrum of trehalose after the addition of the lysozyme to the samples.

3.4. DSC: the effect of LAD processing on the thermal stability of lysozyme

The calorimetric curves of the four samples described in Sect. 2.4 were obtained using DSC. The data was normalized based on the concentration of lysozyme. Figure 11 shows representative calorimetric curves of the samples and the derived thermodynamic properties are given in Table 1.

Biomedical Optics EXPRESS

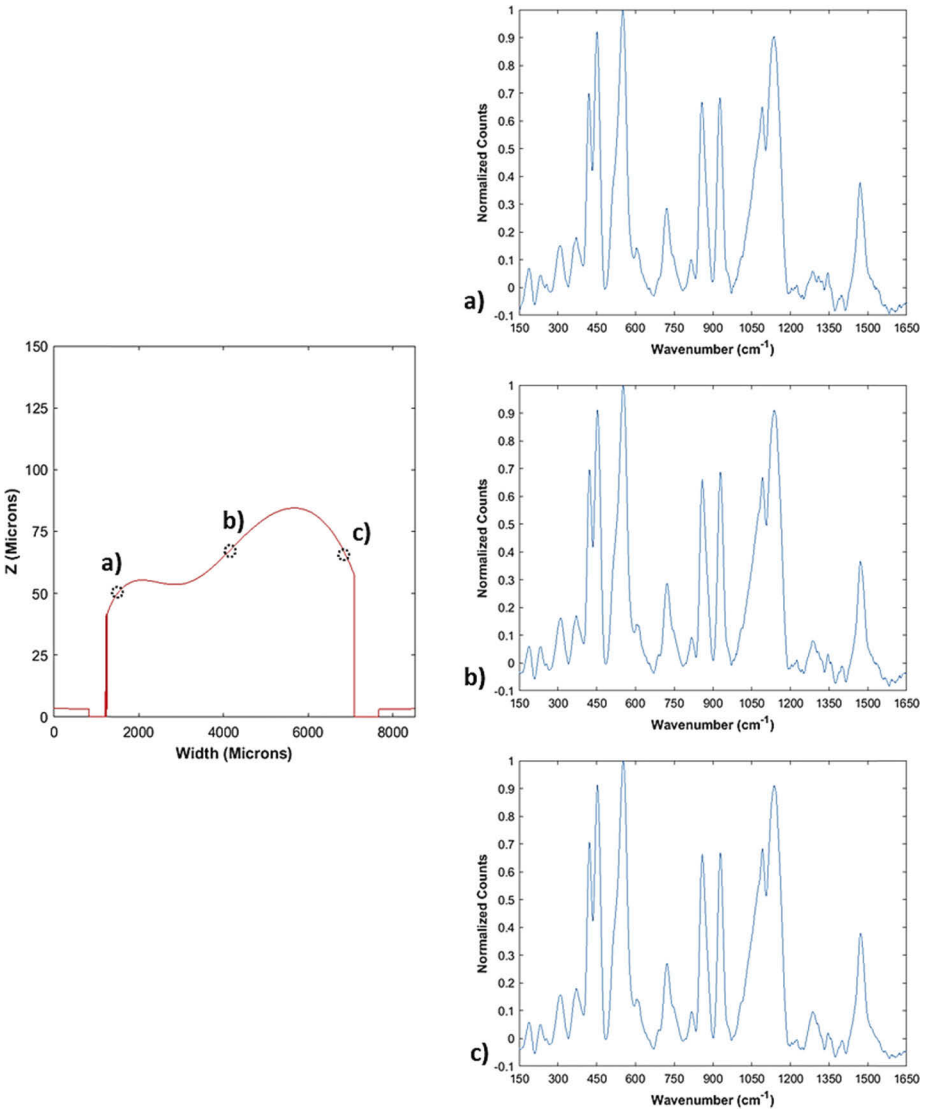

Fig. 10. A SWLI height profile on the left is marked with three locations that correspond to the normalized Raman spectra on the right.

The percent difference for T_m and ΔH as compared to the unprocessed lysozyme are included in Table 1. The changes in T_m and ΔH when compared to the unprocessed control sample are negligible for LAD processing, as well as thermal processing at 43°C and air drying. At the LAD processing temperatures used in this study, no thermal degradation of the lysozyme protein was expected. There was a possibility that the laser radiation could interact with the protein directly and cause unfolding. However, this does not seem to be the case. LAD did not cause any unexpected degradation of lysozyme in the samples. This finding is consistent with our previous study in which the functionality of lysozyme after LAD processing was measured using an assay measuring the rate of lysis of Micrococcus lysodeikticus cells. [13]

Biomedical Optics EXPRESS

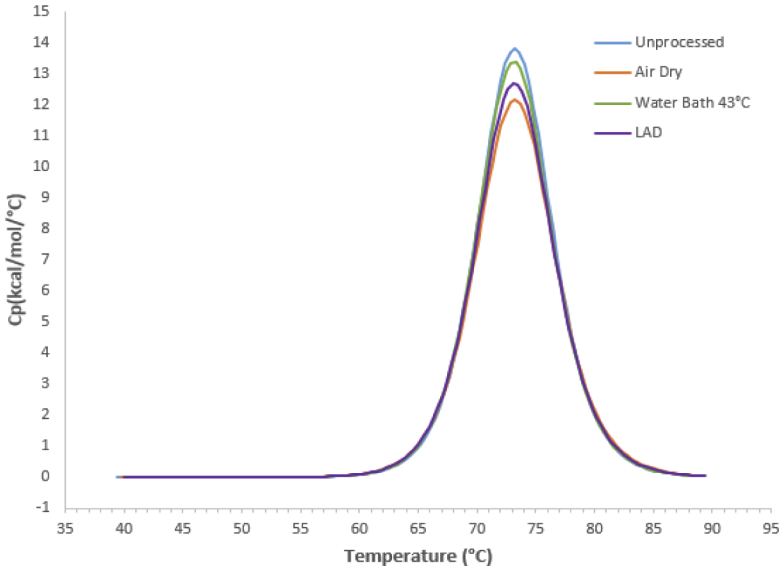

Fig. 11. Calorimetric curves of LAD processed, unprocessed, air dried and thermal processed lysozyme.

Table 1. Thermodynamic parameters for lysozyme as determined with DSC

	T_m (°C)	Change in T_m[a]	ΔH (kcal/mol)	Change in ΔH[a]
Unprocessed (N = 3)	73.20 ± 0.06	—	116 ± 1.9	—
Air Dried (N = 2)	73.29 ± 0.01	−0.12%	106 ± 2.5	8.6%
43°C Water Bath (N = 3)	73.18 ± 0.02	0.03%	112 ± 0.8	3.4%
LAD (N = 2)	73.19 ± 0.02	0.01%	108 ± 1.5	6.9%

[a]Change in thermodynamic parameters compared to the control (unprocessed) sample.

4. Conclusions

This study optically characterized samples processed with LAD using a 1064 nm laser at a maximum processing temperature of ~42°C on borosilicate glass coverslips. We used polarized light imaging to monitor crystallization kinetics of samples immediately post LAD processing and during storage at low RH (14.3 ± 0.5%). LAD processed samples exhibited low initial crystal content. LAD samples experienced a small decrease in EMC when stored at low RH, but did not show the formation of new crystals or growth of crystals during storage. The results of the optical characterization study suggest that LAD processed samples stored at low RH are unlikely to crystallize over a long time scale. Cracking of the samples was discovered near the end of storage. We investigated this cracking with SWLI and determined that it occurred subsurface, likely due to the droplet pulling away from the glass substrate. The use of a more flexible substrate might prevent the cracking. We also used SWLI to show that thickness did not vary substantially across the sample; this has positive implications for solute distribution. Raman spectroscopy showed that there was an even distribution of amorphous trehalose across the sample. SWLI and Raman results imply that samples do have an even distribution of the preservation matrix in an amorphous state which means proteins are more likely to be evenly distributed in their folded state. Finally, we processed a model protein, lysozyme, with the LAD and tested the thermal stability of the processed protein with DSC. The proteins did not show a significant degradation in thermodynamic properties compared to an unprocessed control.

Biomedical Optics EXPRESS

LAD is a more attractive option for anhydrous preservation of proteins compared to lyophilization and other preservation techniques because it is cost effective, relatively fast, can monitor sample temperature during processing and has precise control over energy deposition. In addition, dried samples can be easily rehydrated and recovered from the substrate via pipette. Additional studies still need to be performed to further test the limits of LAD. For example, larger volume samples could be processed using a different laser power, beam size or wavelength as long as the laser radiation could penetrate deeply into the sample to guarantee uniform heating and drying. Future studies would benefit from knowing the spatial EMC to determine a more specific storage temperature range. Along the same lines, only overall average protein functionality was investigated because of the destructive nature of the DSC technique. The spatial distribution and functionality of proteins needs to be determined to further optimize LAD processing. Alternate proteins that are less robust also need to be tested to better understand the effect of LAD on proteins and if the processing temperature is universally applicable to most proteins or if it needs to be optimized on an individual basis. For proteins that denature at lower temperatures, the LAD process can be altered (change in laser power, beam size etc.) to reduce the temperature of the sample during LAD processing. This is an advantage of LAD compared to other stabilization techniques – the process can be easily tuned to appropriate processing conditions for a variety of biologics.

Funding

University of North Carolina at Charlotte (Faculty Research Grants Program, Center for Biomedical Engineering and Science); Charlotte Research Institute Commercial Development Grant Program.

Acknowledgments

The authors would like to thank Dr. Katherine Weaver for her assistance with the DSC measurements and Greg Caskey for his help with the SWLI.

Disclosures

The authors have no relevant financial interests in the manuscript and no other potential conflicts of interest to disclose.

References

1. A. M. Scott, J. D. Wolchok, and L. J. Old, "Antibody therapy of cancer," Nat. Rev. Cancer **12**(4), 278–287 (2012).
2. B. Leader, Q. J. Baca, and D. E. Golan, "Protein therapeutics: a summary and pharmacological classification," Nat. Rev. Drug Discovery **7**(1), 21–39 (2008).
3. V. Romanov, S. N. Davidoff, A. R. Miles, D. W. Grainger, B. K. Gale, and B. D. Brooks, "A critical comparison of protein microarray fabrication technologies," Analyst **139**(6), 1303–1326 (2014).
4. S. F. Kingsmore, "Multiplexed protein measurement: technologies and applications of protein and antibody arrays," Nat. Rev. Drug Discovery **5**(4), 310–321 (2006).
5. E. K. Sackmann, A. L. Fulton, and D. J. Beebe, "The present and future role of microfluidics in biomedical research," Nature **507**(7491), 181–189 (2014).
6. J. Bjerketorp, S. Hakansson, S. Belkin, and J. K. Jansson, "Advances in preservation methods: keeping biosensor microorganisms alive and active," Curr. Opin. Biotechnol. **17**(1), 43–49 (2006).
7. G. D. Adams, "Lyophilization of vaccines: current trends," Methods Mol. Med. **87**, 223–244 (2003).
8. L. Chang, D. Shepherd, J. Sun, D. Ouellette, K. L. Grant, X. Tang, and M. J. Pikal, "Mechanism of protein stabilization by sugars during freeze-drying and storage: Native structure preservation, specific interaction, and/or immobilization in a glassy matrix?" J. Pharm. Sci. **94**(7), 1427–1444 (2005).
9. M. T. Cicerone, M. J. Pikal, and K. K. Qian, "Stabilization of proteins in solid form," Adv. Drug Delivery Rev. **93**, 14–24 (2015).
10. J. H. Crowe and L. M. Crowe, "Preservation of mammalian cells-learning nature's tricks," Nat. Biotechnol. **18**(2), 145–146 (2000).

Biomedical Optics EXPRESS

11. W. F. Wolkers, F. Tablin, and J. H. Crowe, "From anhydrobiosis to freeze-drying of eukaryotic cells," Comp. Biochem. Physiol., Part A: Mol. Integr. Physiol. **131**(3), 535–543 (2002).
12. J. H. Crowe, L. M. Crowe, W. F. Wolkers, A. E. Oliver, X. Ma, J. H. Auh, M. Tang, S. Zhu, J. Norris, and F. Tablin, "Stabilization of dry Mammalian cells: lessons from nature," Integr. Comp. Biol. **45**(5), 810–820 (2005).
13. M. A. Young, A. T. Antczak, A. Wawak, G. D. Elliott, and S. R. Trammell, "Light-assisted drying for protein stabilization," J. Biomed. Opt. **23**(7), 1–8 (2018).
14. D. Champion, M. Le Meste, and D. Simatos, "Towards an improved understanding of glass transition and relaxations in foods: molecular mobility in the glass transition range," Trends Food Sci. Technol. **11**(2), 41–55 (2000).
15. N. Chakraborty, M. A. Menze, H. Elmoazzen, H. L. Vu, M. L. Yarmush, S. C. Hand, and M. Toner, "Trehalose transporter from African chironomid larvae improves desiccation tolerance of Chinese hamster ovary cells," Cryobiology **64**(2), 91–96 (2012).
16. H. Y. Elmoazzen, G. Y. Lee, M. W. Li, L. K. McGinnis, K. K. Lloyd, M. Toner, and J. D. Biggers, "Further optimization of mouse spermatozoa evaporative drying techniques," Cryobiology **59**(1), 113–115 (2009).
17. S. L. Cellemme, M. Van Vorst, E. Paramore, and G. D. Elliott, "Advancing microwave technology for dehydration processing of biologics," Biopreserv. Biobanking **11**(5), 278–284 (2013).
18. M. Young, M. McKinnon, G. Elliott, S. Trammell, D. Levitz, A. Ozcan, and D. Erickson, "Light assisted drying (LAD) for protein stabilization: optical characterization of samples," Proc. SPIE **10485**, 104850W (2018).
19. A. Saleki-Gerhardt and G. Zografi, "Non-isothermal and isothermal crystallization of sucrose from the amorphous state," Pharm. Res. **11**(8), 1166–1173 (1994).
20. N. Chakraborty, D. Biswas, W. Parker, P. Moyer, and G. D. Elliott, "A role for microwave processing in the dry preservation of mammalian cells," Biotechnol. Bioeng. **100**(4), 782–796 (2008).
21. R. W. Hartel and A. V. Shastry, "Sugar crystallization in food products," Crit. Rev. Food Sci. **30**(1), 49–112 (1991).
22. A. A. Evans, E. Cheung, K. D. Nyberg, and A. C. Rowat, "Wrinkling of milk skin is mediated by evaporation," Soft Matter **13**(5), 1056–1062 (2017).
23. B. Sobac and D. Brutin, "Desiccation of a sessile drop of blood: Cracks, folds formation and delamination," Colloids Surf. A Physicochem Eng. Asp. **448**, 34–44 (2014).
24. B. D. Caddock and D. Hull, "Influence of humidity on the cracking patterns formed during the drying of sol-gel drops," J. Mater. Sci. **37**(4), 825–834 (2002).
25. V. Ragoonanan and A. Aksan, "Heterogeneity in desiccated solutions: implications for biostabilization," Biophys. J. **94**(6), 2212–2227 (2008).
26. D. Tuschel, "Molecular Spectroscopy Workbench Why Are the Raman Spectra of Crystalline and Amorphous Solids Different?" Spectroscopy **32**(3), 26–33 (2017).